International Journal of Nanomedicine

Dovepress
open access to scientific and medical research

Open Access Full Text Article

ORIGINAL RESEARCH

Albumin-Modified Gold Nanoparticles as Novel Radiosensitizers for Enhancing Lung Cancer Radiotherapy

Yao Chen[1,*], Shuya Liu[1,*], Yin Liao[1,*], Hanshan Yang[1], Zhuo Chen[1], Yuru Hu[1], Shaozhi Fu[1], Jingbo Wu[1–3]

[1]Department of Oncology, The Affiliated Hospital of Southwest Medical University, Luzhou, People's Republic of China; [2]Nuclear Medicine and Molecular Imaging Key Laboratory of Sichuan Province, Luzhou, People's Republic of China; [3]Academician (Expert) Workstation of Sichuan Province, Luzhou, People's Republic of China

*These authors contributed equally to this work

Correspondence: Shaozhi Fu; Jingbo Wu, Department of Oncology, The Affiliated Hospital of Southwest Medical University, Luzhou, Sichuan Province, 646000, People's Republic of China, Tel/Fax +86 8303165696, Email shaozhifu513@163.com; wjb6147@163.com

Background: Considering the strong attenuation of photons and the potential to increase the deposition of radiation, high-atomic number nanomaterials are often used as radiosensitizers in cancer radiotherapy, of which gold nanoparticles (GNPs) are widely used.
Materials and Methods: We prepared albumin-modified GNPs (Alb-GNPs) and observed their radiosensitizing effects and biotoxicity in human non-small-cell lung carcinoma tumor-bearing mice models.
Results: The prepared nanoparticles (Alb-GNPs) demonstrated excellent colloidal stability and biocompatibility at the mean size of 205.06 ± 1.03 nm. Furthermore, clone formation experiments revealed that Alb-GNPs exerted excellent radiosensitization, with a sensitization enhancement ratio (SER) of 1.432, which is higher than X-ray alone. Our in vitro and in vivo data suggested that Alb-GNPs enabled favorable accumulation in tumors, and the combination of Alb-GNPs and radiotherapy exhibited a relatively greater radiosensitizing effect and anti-tumor activity. In addition, no toxicity or abnormal irritating response resulted from the application of Alb-GNPs.
Conclusion: Alb-GNPs can be used as an effective radiosensitizer to improve the efficacy of radiotherapy with minimal damage to healthy tissues.
Keywords: albumin, gold nanoparticles, radiosensitization, lung cancer, radiotherapy

Introduction

According to the latest global cancer burden data released by the International Cancer Research Agency (ICRA) of the World Health Organization in 2022, lung cancer is the second most malignant tumor for humans, responsible for approximately one-fourth of all cancer-related fatalities, making it a serious threat to the human health and quality of life.[1] Although the available lung cancer treatment tends to be diversified and precise, the treatment effect is not satisfactory. Radiotherapy refers to the use of high-energy ionizing radiation to induce lethal damage to cancer cells, which is critical in the treatment of primary and metastatic solid tumors as well as in inhibiting the metastasis of microscopic tumor and regional lymph nodes. Therefore, radiotherapy is usually applied as one of the primary lung cancer treatments. About 77% of lung cancer patients have evidence-based indications for radiotherapy.[2] In the course of radiotherapy, the maximum amount of radiotherapy must be delivered to the tumor site whenever possible while avoiding damage to normal and healthy tissues, and ultimately improving the treatment outcome. Presently, radiotherapy has entered the era of precision and intelligent therapy, such as application under the guidance of PET and magnetic resonance imaging (MRI) for precise tumor targeting/location and the use of linear accelerators and three-dimensional treatment plans, including stereotactic radiotherapy, intensity-modulated radiation therapy, and the use of charged

Received: 18 November 2022
Accepted: 1 April 2023
Published: 11 April 2023

particles in radiotherapy; these interventions have improved the overall efficacy of radiotherapy.[3] However, the side effects of radiotherapy, including uneven local dose distribution, radiation pneumonitis, myelosuppression after radiotherapy, limited tolerance of normal tissues to high-energy rays, increased tumor resistance to radiotherapy, respiratory mobility, lung infection, and others, significantly limit its application. Interestingly, radiosensitizers seem to be a good choice to improve radiosensitivity.

Currently, a variety of radiosensitizers (such as cisplatin, nitroimidazole, epoxygenase-2 inhibitors, and iodinated DNA targeting agents) have been developed and being applied to tumor radiotherapy. The ideal radiosensitizer should not only enhance the radiotherapy effect of the tumor but also have low toxicity or be non-toxic to the normal tissues, as well as protect the normal tissues.[4] Presently, only a few efficient, non-toxic, low cost, and radiosensitizing materials are available for clinical use. The last few years have witnessed an increasing interest in the use of radiation in conjunction with metal radiosensitizers, thanks to the advancements in tumor therapy.[3,5–8] Moreover, the rapid development in the field of nanomedicine research has provided new therapeutic ideas and strategies. High-atomic number nanomaterials, such as bismuth (Bi, Z = 83),[9] gold (Au, Z = 79),[10,11] tungsten (W, Z = 74),[12] tantalum (Ta, Z = 73),[13–16] hafnium (Hf, Z = 72),[17] and silver (Ag, Z = 47),[18] were able to enrich in tumors tissues by taking advantage of the enhanced permeability and retention (EPR) effects. Nanoparticle (NP) materials containing high Z elements can be applied as radiosensitizers that benefit from the ability of enhancing the absorption cross-section of X-ray, improving the relative dose accumulation of tumors, promoting the generation of free radicals, and enhancing the ability of DNA damage.[19] Among them, gold nanoparticles (GNPs) with a high X-ray photon, which can capture the cross-section of Au, have been widely applied to tumor diagnosis and treatment.[20–24]

Nonetheless, there is much ambiguity about the specific mechanism of radiosensitization of NPs including GNPs, which warrants that the mechanism of radiosensitization be explained and described from the physical, physical chemical, chemical, and biological perspective.[4,22,25,26] Specifically, photoelectrons and Auger electrons resulting from ionizing radiation interacting with GNPs are believed to accumulate large doses at extremely small scales. In addition, based on the physical structure and components of GNPs, solid–liquid phase electron transfer can generate unpaired electrons and promote the dissociation of molecules into free radicals, thereby improving the tumor-killing effect. Regarding the chemical mechanism, the radiosensitization of GNPs mainly improves the tumor cell-killing ability by promoting the production of reactive oxygen species (ROS) and elevating oxidative stress, which mainly depends on the enhancement of the secondary electron output of GNPs to promote hydrolysis. The biological mechanism of radiosensitization in GNPs can be discussed in the following two aspects: the target of inducing radiobiological effects (such as DNA damage) and the influence of the presence of NPs on the radiobiological effects. However, the biological mechanism is influenced by various factors, such as the cell characteristic, the uptake of NPs, and differences between different cell lines.[27] Moreover, a strong and positive correlation can be expected between the tumor local concentration of GNPs and the radiosensitization effect. Regarding GNPs delivery, relying solely on the EPR effect is inadequate to reach an effective concentration. In addition, the NPs directly entering the blood system produce a protein corona, which affects the sensitization effect. Therefore, there is a need to explore the approach to simultaneously achieve radiosensitization by adjusting the local nanoparticle concentration in the tumor.

When compared with the normal cells, tumor cells tend to have a higher rate of albumin metabolism owing to their rapid cleavage and proliferation. Therefore, malignant tumors can transport large amounts of albumin into the lysosomal compartment of cells for decomposition, thereby providing sufficient nutrients and energy for the growth and division of cells. Furthermore, owing to its properties of non-toxic, low immunogenicity, and good biocompatibility and biodegradability, human serum albumin (HSA) has been extensively used as a versatile biocompatible drug-delivery carrier for varied medical purposes.[28–30] The presence of charged amino acid groups in the albumin structure enables it to couple to multiple antitumor drugs. On the other hand, the albumin-based multi-size carrier (from nanoscale to mesoscale) can improve the biodegradability and stability of the drugs and reduce the slow and/or controllable release of the drugs, thereby enhancing the anti-tumor effect of the drugs. Conventional passive targeting can be achieved through the EPR effect, while active targeting using albumin (Alb), as the carrier, has been widely confirmed and applied. Alb-based NPs have high affinity, with the Alb receptor overexpressed on the tumor cell surface (such as gp60) and the cysteine-rich acid secretory protein (SPARC) highly expressed in the tumor stroma that can enhance drug trans-endothelial transport and

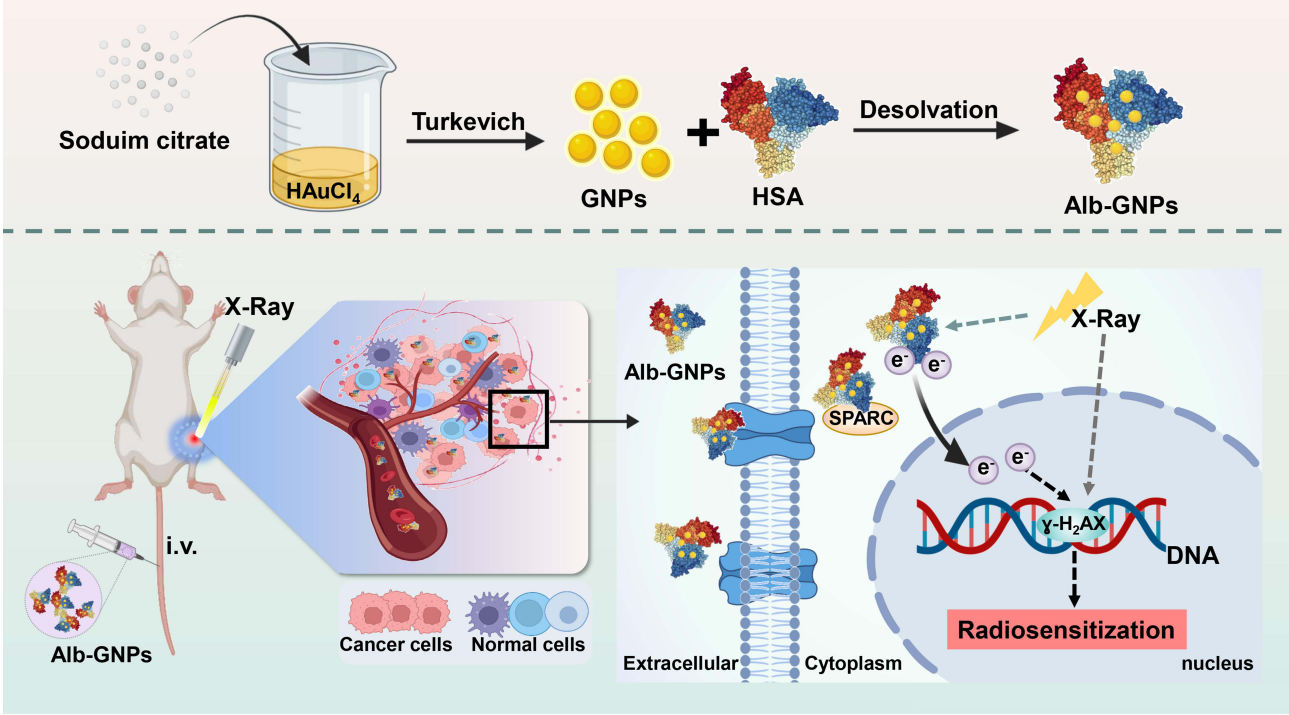

Scheme 1 Schematic illustration of synthesis, radiosensitizing effects and antitumor therapy of Alb-GNPs.

increase the drug concentration in tumor tissues.[31–34] Furthermore, the functionalization of GNPs and the modification of endogenous proteins can increase the blood circulation time, biocompatibility, selective cell uptake, and biodistribution of the NPs.[35,36] Thus, HSA is believed to be an ideal carrier for GNPs delivery.

Accordingly, we aimed to explore novel nanoplatforms for boosting the efficacy of tumor radiotherapy by loading GNPs in Alb-NPs. We employed a simple, low-toxicity method to prepare the composite nanomaterials so as to reduce the accumulation and biotoxicity in the blood system as well as improve the bioavailability of GNPs. We systematically characterized the morphology, particle size, stability, physicochemical properties, and in vitro sensitization-induced antitumor effect of the prepared Alb-modified GNPs (Alb-GNPs). Finally, the nano-composite system was adopted for radiotherapy of a xenografted lung cancer model to further evaluate the radiosensitization effect and toxicity (Scheme 1).

Experimental Section

Materials

Gold acid chloride trihydrate ($HAuCl_4$, >99.99%) was purchased from Sigma-Aldrich (St. Louis, MO, USA). HAS (>96%) was purchased from Hefei Bomei Biotechnology Co., Ltd. (Anhui, China). Sodium citrate tribasic dihydrate ($Na_3C_6H_5O_7$), sodium hydroxide, and absolute ethanol were purchased from Chengdu Chron Chemicals Co., Ltd. (Sichuan, China). N-(3-Dimethylaminopropyl)-N-ethylcarbodiimide hydrochloride (EDC, 98.5%) and D-(+)-Trehalose anhydrous were obtained from Aladdin (Shanghai, China). DMEM, fetal bovine serum (FBS), trypsin-EDTA, and penicillin–streptomycin (P/S) solution were purchased from HyClone (USA). BD Pharmingen 556547 Annexin V FITC Apop Dtec Kit and Anti-gamma $H_2A.X$ (phospho S139) antibody were purchased from Abcam (UK). The In Situ Cell Death Detection Kit was purchased from Roche (USA). Ki-67 antibody was purchased from Bioworld Technology Co., Ltd. (Nanjing, China). All reagents were used without further purification unless otherwise specified. Furthermore, double-distilled deionized water was obtained from a water purification system (Ulupure, China) for use in all experiments.

Lung adenocarcinoma cell line A549 and 5-week-old female BALB/c mice were used in this study. The A549 cells we used were purchased from the Cell Bank of the Chinese Academy of Sciences and provided by the Medical Experimental Center of the affiliated Hospital of Southwest Medical University. All animals are kept in separate cages in specific pathogen-free (SPF) animal

rooms under 12-h photophase and provided with *ad libitum* food and water. The experiments were started after the animals were acclimatized for 1 week.

Experimental Methods

Synthesis of GNPs, Alb-NPs, and Alb-GNPs

For the preparation of GNPs, a modified Turkevich method was employed. Briefly, 24 mg of $HAuCl_4$ was dissolved in 50 mL of double-distilled water and boiled. Subsequently, 5 mL of sodium citrate solution (4 mg/mL) was quickly added to this solution under vigorous stirring. The resultant solution was kept under reflux for 2 h under continuous vigorous stirring. The color of the solution eventually changed to wine-red, indicating the successful preparation of GNPs. The GNPs solution was further purified and centrifuged with a centrifugal filter (Allegra 64R) three times (14,000 rpm, 20–30 min), followed by storage in the freezer until further use.

The preparation of Alb-NPs was performed according to the desolvation technique, albeit with some modifications.[30] Briefly, 100 mg of HSA was dissolved in 4 mL of H_2O, the pH was adjusted to 8.0–9.0 (1 M NaOH). Then, the excess ethanol was added dropwise (1–2 mL/min) to the HSA solution under constant stirring at room temperature. The addition of ethanol was stopped when the solution turned turbid. For stabilizing the NPs, EDC (0.5 mL, 10 mg/mL) was added to this solution for cross-linking. The resultant solution was then continuously stirred for 3 h at room temperature to ensure the cross-linking of all amino acid residues. The color of the solution changed from transparent to slightly blue opalescent, indicating the successful preparation of the Alb-NPs. Then, the prepared solution was solidified overnight at 4°C. The desolvation method was also performed for the synthesis of Alb-GNPs, except that the HSA solution was mixed with an appropriate amount of GNPs solution before adding ethanol. Subsequently, the suspension was subjected to ultrafiltration (dialysis, MW: 3500 Da) for 4 h to remove the free Alb-NPs and GNPs. Finally, the nanosuspension was freeze-dried with 6% trehalose as a cryoprotectant agent to obtain a fine powder of the NPs and stored at 4°C until required.

Characterization of GNPs, Alb-NPs, and Alb-GNPs

The sizes, zeta potential, and polydispersity index (PDI) of GNPs, Alb-NPs, and Alb-GNPs were measured by using a particle size analyzer (NanoBrook 90 Plus Zeta, Brookhaven, NY, USA) at a 90° scattering angle through dynamic light scattering. The morphology and microstructure of GNPs and Alb-GNPs were analyzed by transmission electron microscope (TEM; Tecnai G2 F20, USA). Furthermore, the comparative investigation on the UV-Vis spectral analysis of absorbance of GNPs, Alb-NPs, and Alb-GNPs was performed in the wavelength range of 400–800 nm with the UV-5800PC (Shanghai, China). The Au concentrations of GNPs and Alb-GNPs solutions were determined by inductively coupled plasma spectroscopy (ICP-OES, Agilent, USA).

Cellular Uptake

When A549 cells were grown to 80% confluence in culture flasks, they were digested and seeded into 6-well plates (1×10^5 cells/well) for 24 h. The complete medium in each well was then replaced with different concentrations (0, 10, 20, and 30 mg/mL) of Alb-GNPs (dissolved in DMEM). After incubation for 24 h, the cells were washed thrice with PBS (0.01 M, pH = 7.4) to remove the non-internalized NPs and then observed with a fluorescence microscope (Leica TE2000-S Microscope, Olympus, Tokyo, Japan).

Cytotoxicity and Cell Survival Experiments

To examine the cytotoxicity of Alb-GNPs, the typical MTT assay was performed. Briefly, A549 cells were seeded in 96-well plates (8×10^3 cells/well) for overnight. The culture medium was then removed, and the cells were incubated with different concentrations of the Alb-GNPs solution (0–50 mg/mL) for 24 h, followed by the addition of 20 μL MTT solution (5 mg/mL). After further incubation for 4 h, the liquid in the well plates was removed and 150 μL of DMSO was added. The absorbance was measured and recorded at 490 nm with a microplate reader (iMark, BioRAD, USA).

For the cell survival experiments, A549 cells were seeded in 96-well plates as per the abovementioned method and incubated overnight. After replacing the medium with 100 μL of the Alb-GNPs solution of different concentrations (0–50 mg/mL), the plates were incubated for another 24 h. After removing the solution in the 96-well plate, an equal amount of the incomplete medium was added and placed under a linear accelerator (Elekta, Sweden) for irradiation (source skin distance (SSD): 100 cm, dose rate: 200 cGy/min). The single exposure doses were 0, 2, 4, 6, and 8 Gy, respectively. Next, the cells were incubated for another 24 h, after

which the MTT solution and the DMSO solution were added, followed by a reading of the absorbance at 490 nm with a microplate reader.

Clonogenic Assay

First, A549 cells were seeded at an appropriate density in 6-cm petri dishes and incubated overnight. Then, the cells were incubated with the Alb-GNPs solution of different concentrations (10, 20, and 30 mg/mL) for 24 h, and the petri dishes were gently washed with sterile normal saline to remove the non-internalized NPs and incubated with fresh culture medium. The prepared cells were subjected to 6-MV X-ray for irradiation as soon as possible with radiation doses of 0, 2, 4, 6, and 8 Gy in a single fraction. Subsequently, the cells were replanted at a lower density in petri dishes and incubated for 14 days. The culture was terminated when the cell clusters became visible to the naked eye. The cells were washed and fixed with formaldehyde and then stained with 1% crystal violet. ImageJ software was used to enumerate the colonies, and each colony contained at least 50 cells. The plating efficiency, survival fraction (*SF*), and other radiobiological parameters, including average lethal dose (D_0), quasi-threshold dose (D_q), and sensitization enhancement ratio (SER), were calculated. The single-hit multi-target model was measured to fit the dose–survival curve.

Cell Apoptosis and Cell Cycle in vitro

To further demonstrate the anti-tumor effect and the radiosensitization effect of Alb-GNPs combined with radiotherapy, cell apoptosis, and cell cycle detection were performed. A549 cells (1×10^6 cells/well) were seeded into 6-well plates and incubated overnight, followed by exposure to different concentrations (10, 20, and 30 mg/mL) of the Alb-GNPs solutions for 24 h, replacement with the fresh medium, and subjection to X-ray irradiation with the different radiation doses. Subsequently, the cells were incubated for 24 h.

For the cell apoptosis analysis, the cells and supernatant were collected after different treatments, centrifuged at 1000 rpm for 2 min, and the cell precipitates were collected. The cells were then resuspended in 100 μL of 1× binding buffer, followed by the addition of Annexin V-FITC (5 μL) and propidium iodide (PI, 5 μL) staining solution. The solution in each flow tube was mixed well and incubated at room temperature in the dark for 30 min.

For cell-cycle analysis, the treated A549 cells were collected and fixed with 70% ethanol at 4°C overnight. The cells were resuspended in PBS and then centrifuged at 1500 rpm for 5 min. The cell precipitates were collected, treated with 100 μL RNase A solution, incubated at 37°C for 30 min, and stained with 400 μL of the PI staining solution at room temperature for 20–30 min in the dark.

All samples were detected and analyzed according to the kit guidelines by flow cytometry (DxFlex Flow Cytometry, Beckman Coulter, USA).

In vivo Antitumor and Radiosensitization Effect

All animal experiments were approved by the Laboratory Animal Ethics Committee of Southwest Medical University and conducted in accordance with the animal care guidelines of the Institutional Animal Care and Treatment Committee of Southwest Medical University. All procedures were performed under sterile conditions.

To establish the tumor xenograft model, Balb/c female nude mice (5 weeks, 17–18 g) were subcutaneously injected in the right thigh within 0.1 mL of A549 cells (1×10^7 cells). When the average subcutaneous tumor volume reached 80–100 mm^3, these mice were assigned to the following 6 groups (n=10) randomly: 1) Control (0.9% normal saline, NS); 2) GNPs; 3) Alb-GNPs; 4) X-ray (a single dose of 6 Gy); 5) GNPs + X-ray; 6) Alb-GNPs + X-ray. Alb-GNPs (50 mg/mL) and GNPs (the same amount of Au content) were injected into mice, then the mice were exposed to 6 Gy of X-ray radiation (6 MV, SSD: 100 cm, dose rate: 200 cGy/min).

All treatments were administered only once, and the mice were observed daily. The mice's body weights, tumor length, and tumor width were monitored every 2 days.

Biodistribution of GNPs

The tissue distribution was detected after 24 h of injection of GNPs and Alb-GNPs. The tumor tissues and important organs (such as the liver, lung, and kidney) of the mice were collected, weighed, and ablated in an aqua regia solution for 4 h. The mice injected

with NS served as negative controls. The Au content in each tissue sample was determined by inductively coupled plasma-atomic emission spectroscopy (ICP-AES).

In vivo Toxicity Evaluation and Immunohistochemical Analysis

The tumor tissues from the mice in different groups were collected within 48 h of treatment for γ-H2AX detection by immunohistochemistry (IHC). After treatment, nude mice were randomly sacrificed, their important organs (such as the heart, liver, spleen, lung, and kidney) and tumor tissues were collected after treatment for histopathological observation, including H&E staining and other indicators of IHC (ie, Ki-67, and TUNEL). In addition, the blood from mice was collected within 48 h of treatment for hematological toxicity analysis.

Statistical Analysis

All experimental data were presented as the mean ± standard deviation (SD). Statistical analysis was performed by using the statistical package SPSS 22.0 (Chicago, IL, USA) using Student's test for two-group comparison or one-way ANOVA for multiple-group comparison. Kaplan–Meier survival was used to analyze the survival rate of mice. $P < 0.05$ was considered to indicate statistical differences. All charts in the experiment were illustrated using Prism 8.0 (GraphPad, La Jolla, CA, USA) and SigmaPlot 14.0 (Systat Software Inc, San Jose, CA, USA).

Results

Preparation and Characterization of NPs

We successfully synthesized 3 types of NPs (GNPs, Alb-NPs, and Alb-GNPs). As Figure 1A suggests, the GNPs solution appeared wine-red, the Alb-NPs aqueous solution faint-blue color, and the Alb-GNPs solution as amaranth color. The hydrodynamic diameter, zeta potential, and PDI of these 3 NPs are shown in Table 1, among them, the average

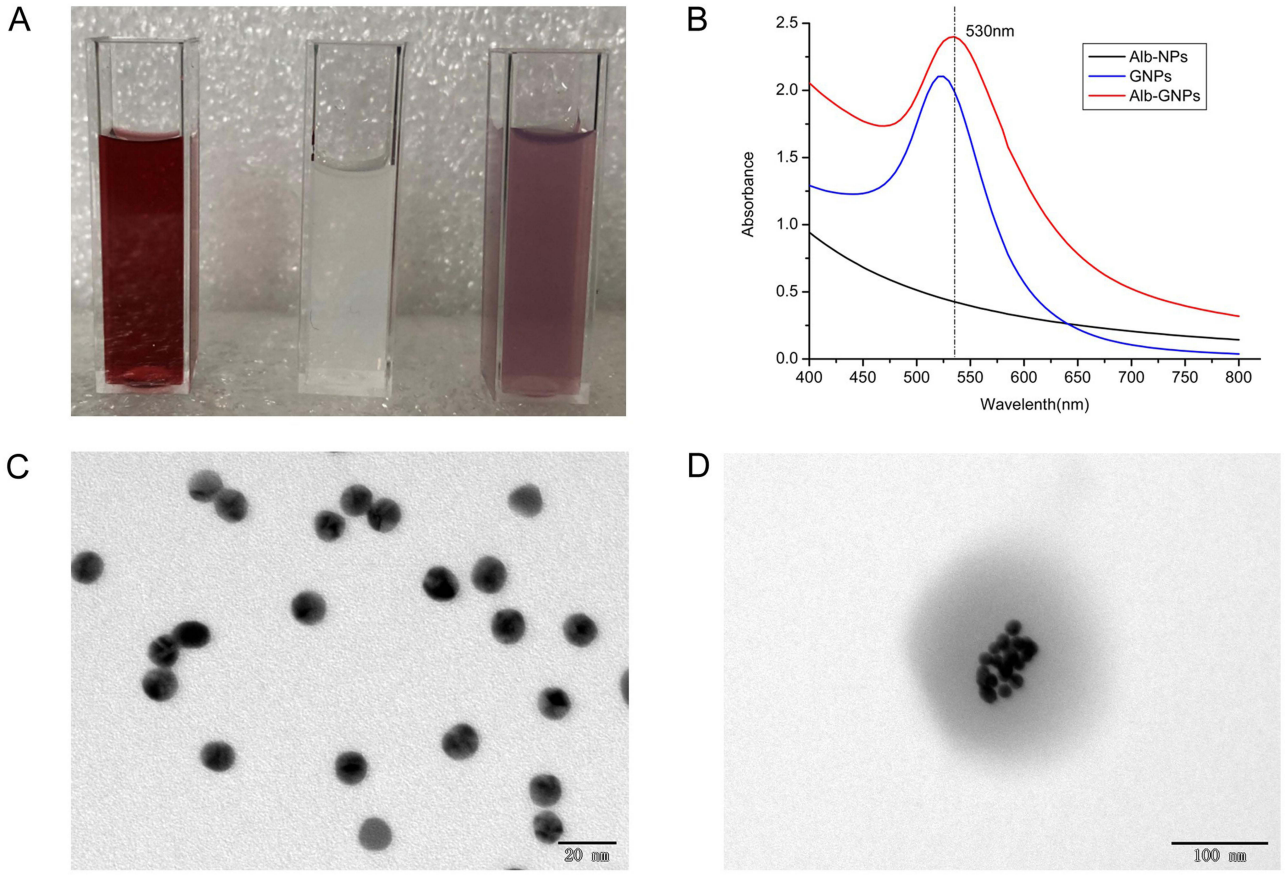

Figure 1 Characterization of GNPs, Alb-NPs and Alb-GNPs in vitro. (**A**) Aqueous solution of GNPs (left), Alb-NPs (middle) and Alb-GNPs (right), respectively. (**B**) The wavelength of GNPs, Alb-NPs and Alb-GNPs, respectively. (**C**) TEM images of GNPs. (**D**) TEM images of Alb-GNPs.

Table 1 Characterization of Nanoparticles

Samples	Particle Size (nm)	PDI	Zeta Potential (mV)
GNPs	23.61±0.40	0.18±0.01	−22.64±2.16
Alb-NPs	105.34±0.40	0.16±0.01	−21.25±2.02
Alb-GNPs	205.06±1.03	0.08±0.02	−32.12±0.31

Note: Date were represented as mean ± SD (n=3).
Abbreviations: GNPs, gold nanoparticles; Alb-NPs, albumin nanoparticles; Alb-GNPs, albumin-modified gold nanoparticles; PDI, polydispersity index.

hydrodynamic diameter of Alb-GNPs was 205.06 ±1.03 nm. The successful fabrication of Alb-GNPs was also confirmed by UV-vis spectroscopy measurements (Figure 1B): no absorption peak was observed for Alb-NPs at the wavelength range of 400–800 nm, while a slight right shift of the absorption peak location was recorded for Alb-GNPs (peak at 530 nm) when compared with GNPs (peak at 525 nm). GNPs and Alb-GNPs were uniform and monodispersable, as characterized by TEM (Figures 1C and D). Furthermore, the Au concentrations of GNPs and Alb-GNPs were 146.7 mg/L and 11.945 g/kg, respectively.

Cytotoxicity, Cell Survival Assay, and Cellular Uptake

MTT assay results shown in Figure 2A indicate that Alb-GNPs exhibited >90% cell viability at all concentrations used (0–50 mg/mL), suggesting no evident cytotoxic effect of Alb-GNPs. Furthermore, we investigated the effects of different concentrations of Alb-GNPs combined with different doses of X-rays on cell viability. With reference to Figure 2B, the cell survival rate decreased gradually with increasing radiation dose and the concentrations of Alb-GNPs.

The results of cellular uptake are depicted in Figure 2C, and Alb-GNPs could be effectively ingested by A549 cells after 24 h of incubation, showing an increased concentration of Alb-GNPs and increased cellular uptake. With increasing Alb-GNPs concentration, the intracellular fluorescence intensity also strengthened, suggesting increased cellular uptake.

The Radiosensitization Effect Conferred by Alb-GNPs

The survival fraction of each group is illustrated in Figure 3, and the radiobiological parameters of each group (Supplementary Table 1) were calculated by clicking on the single-hit multi-target model to fit the experimental data. As suggested by the aforementioned results, the survival fraction decreased with increasing radiation dose and the concentration of Alb-GNPs. The heavy concentration of Alb-GNPs combined with radiation displayed an evident reduction in colony formation when compared with X-ray results alone, which generated the highest SER of 1.432. This result indicated that Alb-GNPs could serve as an effective radiosensitizer in radiotherapy in vitro.

In vitro Antitumor and Radiosensitization Effect

Apoptosis and cell-cycle distribution served as important indicators to evaluate the antitumor effect in vitro. In general, the apoptosis rate increased with an increase in the concentration of Alb-GNPs and the dose of radiotherapy (Supplementary Figure 1 and Supplementary Table 2). However, the application of high-concentration Alb-GNPs with radiotherapy showed no significant difference in the apoptosis rate between 6 Gy and 8 Gy (52.83 ± 0.92% vs 53.09 ± 1.56%, $P > 0.05$) (Figure 4A). Considering the side effects of radiotherapy, we adopted 6 Gy as the dose of radiotherapy in the subsequent experiments.

The difference in cell-cycle distribution between each group was mainly manifested as the percentage of cells in the G2/M phase (Supplementary Figure 2 and Supplementary Table 3). As can be seen in Figure 4B, the percentage of cells in the G2/M phase increased with an increase in the nanoparticle concentration and radiation dose. No significant differences were recorded in the S phase ($P > 0.05$ in all groups).

Body Distribution Detection

ICP-AES was used to quantify the Au element in the major organs and tumor tissues of mice. The distribution and content of Au in each group of mice are shown in Figure 5E. For the tumor tissues, the Alb-GNPs group showed the

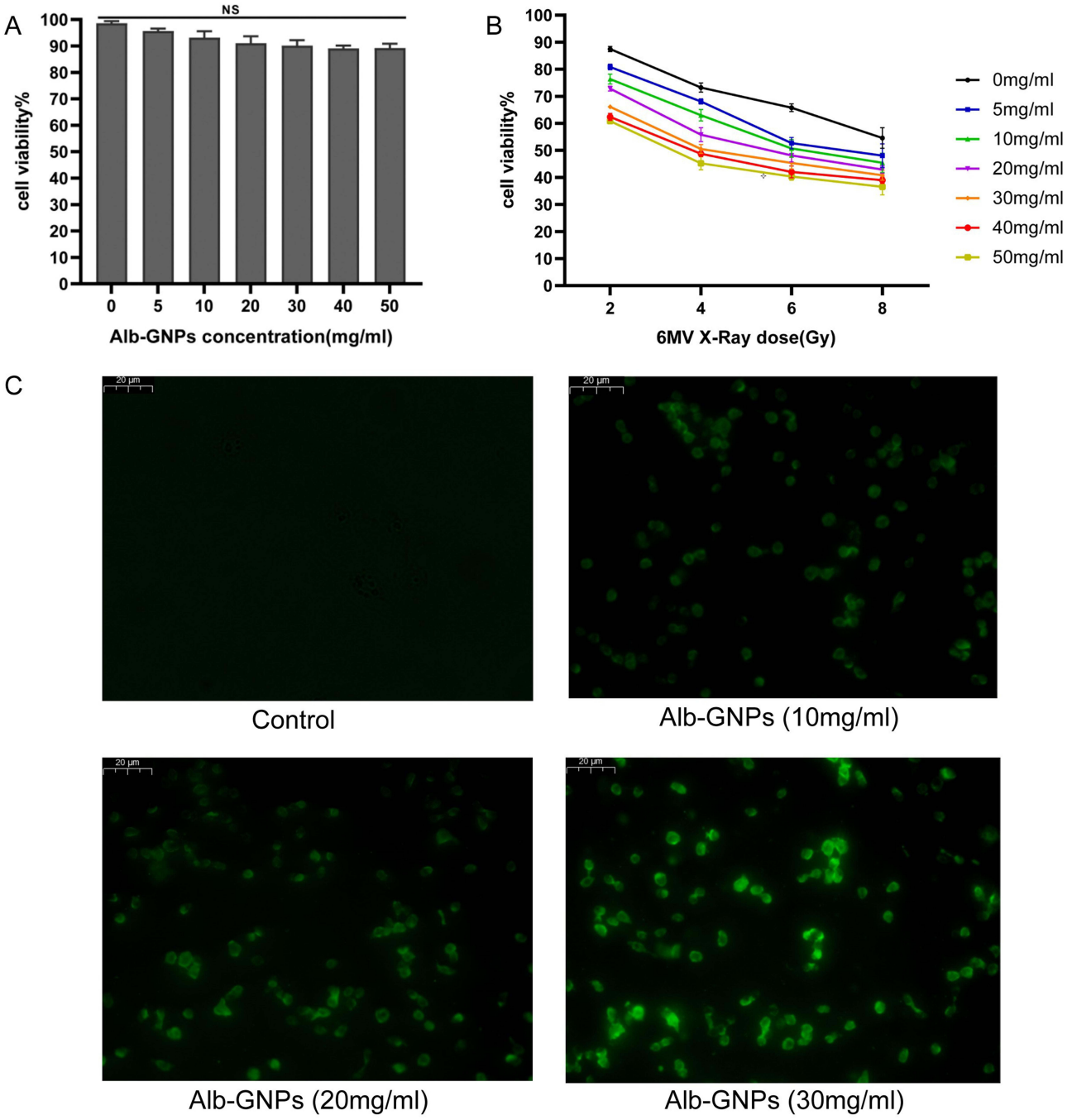

Figure 2 Cytotoxicity assessment and fluorescent images of cell uptake experiments in vitro. (**A**) Cell viability under different concentration of Alb-GNPs for 24 h. (**B**) Cell viability under different concentrations of Alb-GNPs combined with different dose of 6MV X-ray. (**C**) Fluorescent images of A549 cells treated with different concentrations of Alb-GNPs for 24 h, bar=20 μm.
Abbreviation: NS, not statistically significant.

highest Au content relative to the control group and the GNPs group, indicating that Alb-GNPs could be effectively taken up by the tumor tissues. In addition, for other organs (such as the liver, spleen, lung, and kidney), the Au content in the liver and spleen tissues of both the Alb-GNPs and GNPs groups were higher than that of the control group, possibly in association with their metabolic pathways.

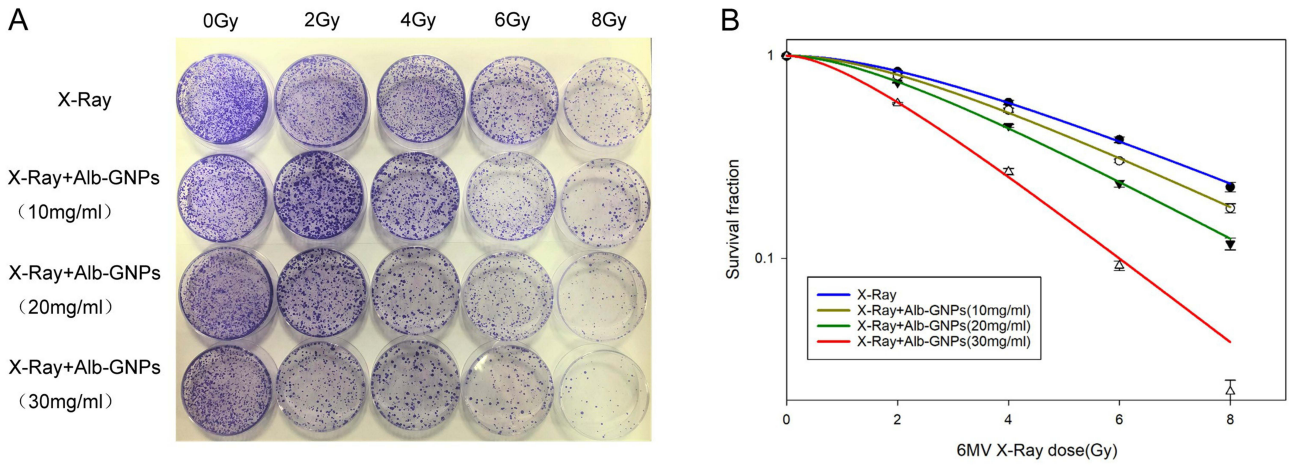

Figure 3 Clonogenic formation experiments in vitro. (**A**) Colony formation in X-ray (6 MV) and different concentrations (10, 20, 30 mg/mL) of Alb-GNPs combined with X-ray (6 MV). (**B**) Survival fraction of X-ray (6 MV) and different concentrations (10, 20, 30 mg/mL) of Alb-GNPs combined with X-ray (6 MV).

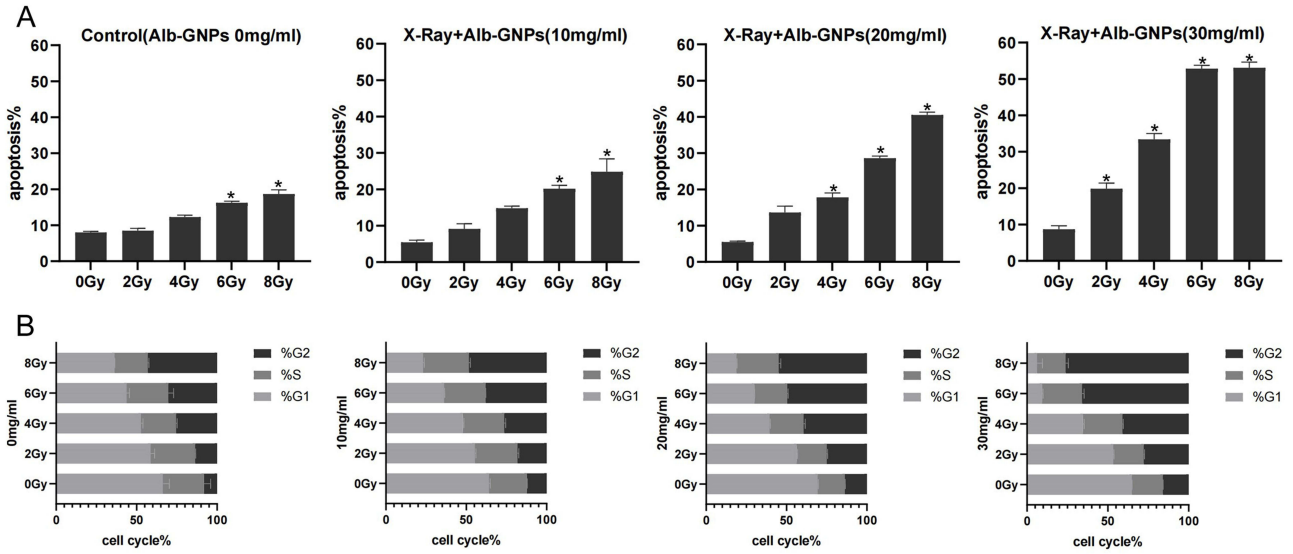

Figure 4 Apoptosis analysis and cell cycle distribution of A549 cells in each group in vitro. (**A**) The rate of cell apoptosis of different treatment groups, *p<0.05. (**B**) Cell cycle distribution of A549 cells for different treatment groups (P<0.05 in all cases).

In vivo Radiosensitization Verification

To evaluate the antitumor therapy effect in vivo, the average tumor volumes of different groups were calculated and the tumor growth curve was drawn accordingly (Figure 5B). As illustrated, the tumor volume increased fastest in the control group and slowest in the Alb-GNPs+X-Ray group ($P < 0.05$), suggesting that the combination of Alb-GNPs and radiotherapy was more effective in delaying tumor growth; this result is consistent with the general view about tumor tissues (Figure 5A). In addition, no obvious change was noted in the tumor volume between the GNPs and Alb-GNPs groups. Meanwhile, we determined the median survival time of each group of mice to assess for a similar effect between each group (Figure 5D). The median survival time of mice in the Alb-GNPs+X-ray group (47.80 ± 7.19 days) was found to be significantly longer when compared to that in the mice treated with GNPs+X-ray (39.60 ± 5.13 days), X-ray (35.60 ± 3.97 days), Alb-GNPs (32.40 ± 3.65 days), GNPs (32.60 ± 4.45 days), and control group (29.40 ± 3.36 days). These results indicated that the combination of Alb-GNPs with radiotherapy could prolong the survival period of the tumor-bearing mice. During our experimental observation, no significant differences were noted in the body weight of the mice between each group (Figure 5C).

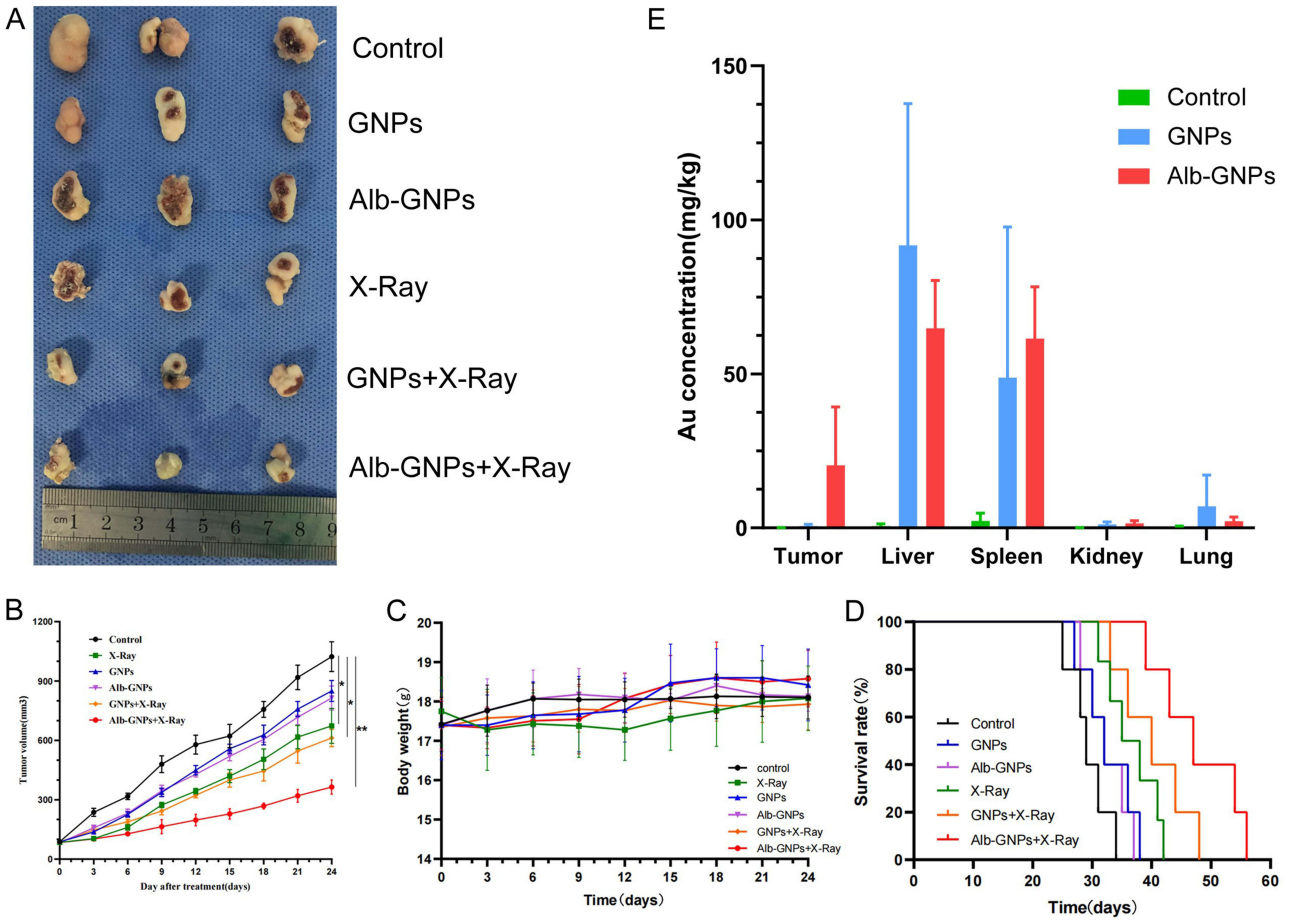

Figure 5 Evaluation of antitumor efficiency in vivo and body distribution. (**A**) General view of tumor tissue with different treatments; (**B**) tumor growth curves for the different experimental groups (*p<0.05, **p<0.01). (**C**) Body weight changes of mice during the period of the experiment. (**D**) The survival rate of each group. (**E**) The Au concentration in tumor, liver, spleen, kidney, and lung tissue of different groups.

Immunohistochemical Analysis

The immunohistochemical results revealed the potential radiosensitization mechanism of Alb-GNPs. Further γ-H2AX-staining images of the tumors (Figure 6A) and quantitative analysis of γ-H2AX-positive cell percentages (Figure 6B and Supplementary Table 4) suggested that the brown signals representing the γ-H2AX-positive proliferative cells led to the most significant increase in the Alb-GNPs+X-ray group. Moreover, the proportion of γ-H2AX-positive cells in the Alb-GNPs+X-Ray group was 79.58% ± 2.83%, which is significantly higher than that of GNPs+X-ray (55.41% ± 3.04%) and single X-ray (40.52% ± 3.81%) groups and all other non-X-ray groups ($P < 0.05$).

Ki-67, a cell proliferation index, can reflect the activity of cell proliferation. The proportion of Ki-67-positive cells in the Alb-GNPs+X-ray group was 25.84 ± 2.05%, which indicated an obvious decrease in the cell proliferation rate when compared to that of the GNPs+X-ray (39.82 ± 3.13%), X-ray (56.27 ± 2.95%), and other treatment groups ($P < 0.05$) (Figure 6C and Supplementary Table 4).

Finally, the TUNEL assay was performed. In this assay, single apoptotic bodies or apoptotic cell nuclei are stained in situ, which accurately reflects the apoptosis situation. As illustrated in the TUNEL-staining images (Figure 6A) and quantitative cell apoptosis rate analysis (Figure 6D and Supplementary Table 4), the Alb-GNPs+X-ray (60.03 ± 4.58%) induced much more apoptotic tumor cells than GNPs+X-ray (46.16 ± 3.42%) and X-ray alone (35.07 ± 3.63%) and other treatments without X-ray ($P < 0.05$).

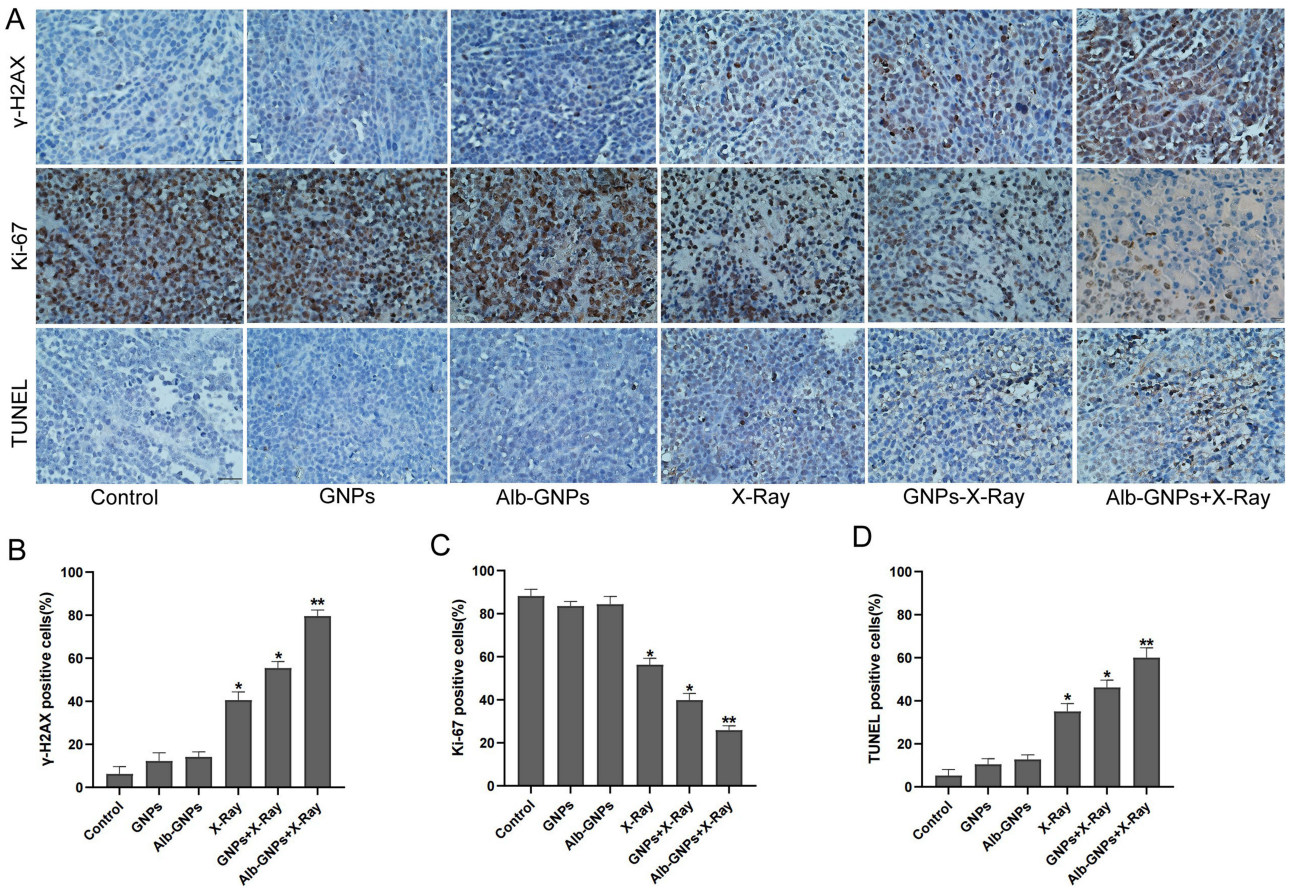

Figure 6 Immunohistochemical analysis of tumors. (**A**) Representative images of IHC of each group for the evaluation of γ-H2AX, Ki-67, and TUNEL (magnification ×400). (**B**) Quantitative analysis of γ-H2AX in tumors from mice in each group. (**C**) Quantitative analysis of Ki-67 in tumors from mice in each group. (**D**) Quantitative analysis of TUNEL in tumors from mice in each group (*p<0.05, **p<0.01). Alb-GNPs + X-ray group resulted in a significantly increase in the expression of γ-H2AX and TUNEL, while a decrease in Ki-67.

Evaluation of in vivo Toxic Side Effects of NPs

Based on the experimental results, with respect to the blood toxicity parameters, we detected no corresponding blood changes in the blood samples of different groups of mice after applying the different treatment strategies (Supplementary Table 5), such as leukopenia and damage of the liver and kidney functions. Moreover, the resultant pathological changes were examined by H&E staining (Figure 7), suggesting varying degrees of tumor cell death in the mice group exposed to simple radiotherapy and NPs combined with radiotherapy, while the most distinctive tumor necrosis was recorded in the Alb-GNPs+X-ray group. Similarly, as illustrated in Figure 7, no appreciable organ damage and pathological abnormalities were recorded in the H&E-stained sections of the heart, liver, spleen, lung, and kidney organs in all treatment groups.

Discussion

Developing an effective radiosensitization system to alleviate or resolve radioresistance to tumor radiotherapy is critical. Radiosensitization can be cons Developing an effective radiosensitization system to alleviate or resolve radioresistance to tumor radiotherapy is critical. Radiosensitization can be considered a process through which radiosensitizers present inside the tumor interact with irradiation and/or biological targets in order to optimize the effect of radiotherapy. Owing to its critical role in the treatment of most cancers, it has also been regarded as "the new dogma of cancer treatment".[20] An ideal radiosensitizer should have the following characteristics: 1) a high sensitization enhancement rate; 2) good tumor-targeting ability and low accumulation in the normal tissues; 3) good biocompatibility or low toxicity; and 4)

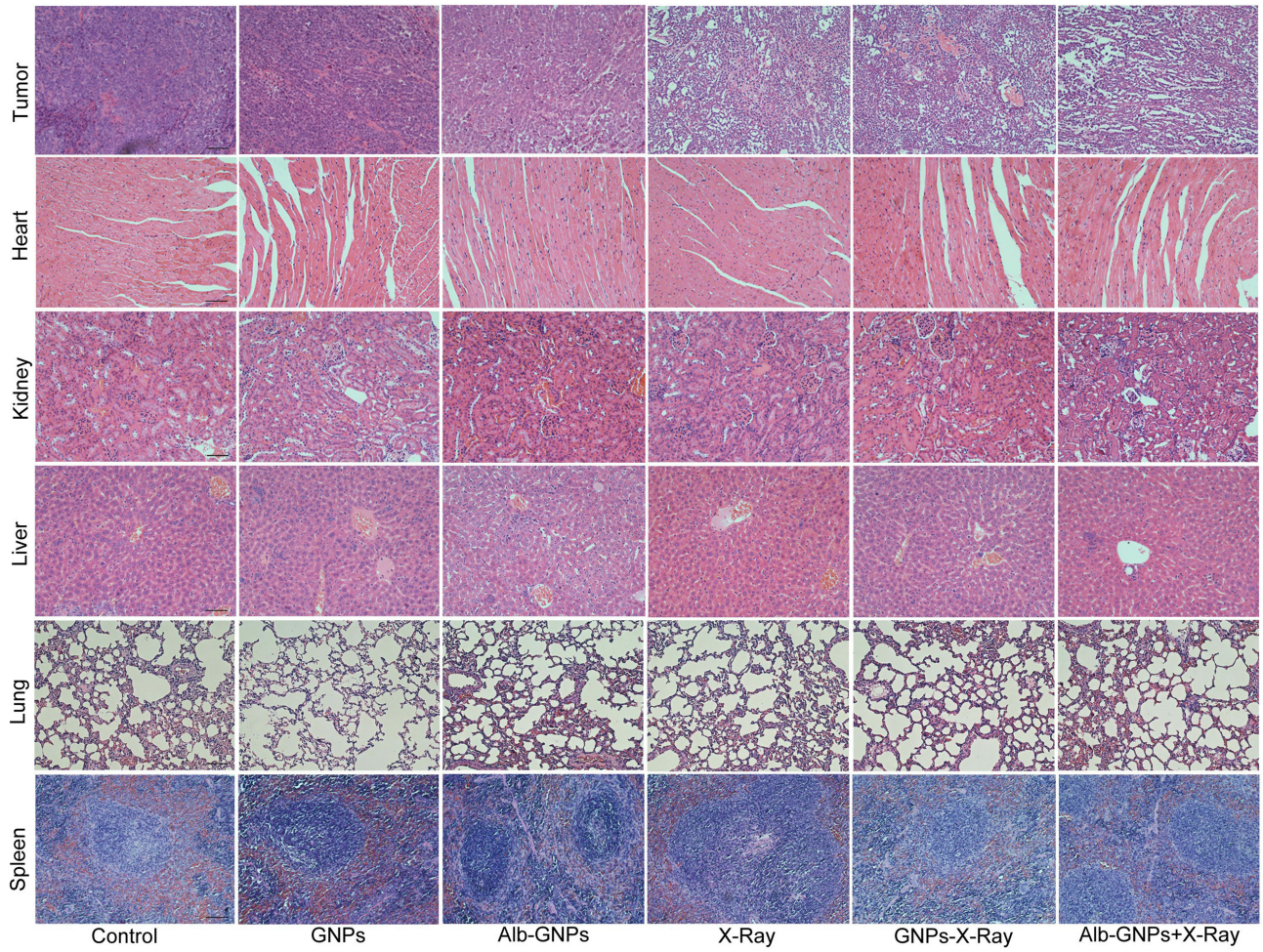

Figure 7 H&E staining of tumor tissues and vital organs in each group (magnification, ×200).

effective renal clearance to avoid potential short-term and long-term toxicity to the human body. However, such ideal radiosensitizer has not yet been developed.[7,37]

Presently, the commonly used radiosensitizers include chemotherapy drugs, gas molecules, and high Z elements. Chemical radiosensitizers, such as platinum analogues and tyrosine kinase inhibitors, belong to a class of commonly used radiosensitizers. They can enhance radiotherapy by regulating the cellular responses, such as reducing radiation resistance of tumor cells, slowing down neovascular production or destroying tumor blood vessels, and inducing cell apoptosis and inhibiting DNA repair. Although the effectiveness of these chemical radiosensitizers has been confirmed previously, their cytotoxicity and side effects cannot be overlooked, which includes myelosuppression, gastrointestinal reaction, and neurotoxicity.[38] In addition, the targeted yield/cellular uptake of radiosensitizers is crucial for radiotherapy enhancement. Chemical radiosensitizers are also limited by the drug concentration. Gas radiosensitizers, such as O_2, NO, and H_2S, enhance the effect of radiotherapy by increasing the reactive oxygen species (ROS) production and/or reducing the expression of hypoxia-inducible factor-1α (HIF-1α). However, the therapeutic efficacy could not be ensured due to the difficulty in controlling the concentration, diffusion rate, and retention time of gas molecules at the tumor site.[39]

As an alternative option, metal-based nanomaterials, especially high-Z materials (eg, Au, bismuth, platinum, gadolinium), have been used in experimental and clinical applications as common radiosensitizers.[40–42] Owing to the emission of low-energy photoelectrons and the interaction of Auger electrons, high-Z nanomaterials can absorb, scatter, and eradicate radiation energy. Moreover, when compared with other metal-based nanomaterials, Au-based nanomaterials are most widely used for this purpose, owing to the following advantages it offers: 1) a strong X-ray attenuation

capability that makes it suitable for use in computer tomography (CT) imaging contrast agent and radiosensitizer[43–45]; 2) as it can be easily surface-modified and embedded in structures such as liposomes and polymer particles, it is frequently used in different tumor treatment protocols; 3) as an inert metal, it exhibits good biocompatibility and low biotoxicity.

Different physicochemical parameters of GNPs, such as size, shape, surface coating and surface charge, can have different effects on cellular uptake, cellular biological response and their interaction with ionizing radiation.[46] Over the years, several studies have been conducted to apply different shapes of Au-based nanomaterials in tumor treatment. In contrast, gold nanoparticles are deemed more suitable for radiosensitization than gold nanorods, which is why we selected GNPs. Generally, the NPs can penetrate the tumor tissues through the EPR effect. However, simple NPs are easily captured by the reticuloendothelial system during blood circulation; furthermore, reaching the tumor site does not guarantee efficient intratumoral penetration or adequate intratumoral concentration. Poor penetration can create an insufficient drug concentration in tumors, which is one of the important reasons for the development of drug resistance and tumor treatment failure.[34,47] Therefore, it is difficult for GNPs to satisfy the long-term tumor retention and rapid clearance in other tissues in vivo, which could increase the efficiency and improve the specificity of radiotherapy. In addition, the different sizes of nanomaterials display different characteristics in drug delivery: NPs <10 nm are easily removed by the kidney, which reduces the circulation time and tumor accumulation, while small-sized NPs may still flow back into the blood circulation after penetrating the tumor, thus spreading to the surrounding tissues and restricting enrichment in the tumor focus for a long time. Although the NPs of 10–100-nm size range have a long blood circulation time and can accumulate in the tumor tissues through EPR effect, the phagocytosis of the liver, kidney and other organs remains the main obstacle, resulting in unsatisfactory cumulative tumor cumulative dose and adding to the difficulty in achieving a therapeutic effect.[37] In this situation, surface modification can serve as an eligible candidate.

In the drug-delivery systems, multiple materials have been used for drug surface modification in order to enhance the therapeutic effects and minimize the toxic side effects. As the most abundant plasma protein, HSA has found an increasingly wide range of applications as an ideal drug delivery carrier, and it can isolate inorganic ions through biomineralization in an alkaline environment to form protein-coated metal oxide nanoclusters.[48–50] Considering the possibility of late clinical switching and clinical application, we selected HSA for coating the modification of GNPs, but not bovine serum albumin (BSA), although they share 75.6% of sequence identity. And compared with HSA, intravenous injection of BSA may cause mild immune response. NPs modified with Alb can achieve longer blood circulation time and lower blood toxicity. Their accumulation in the tumors can be attributed to the effective interaction of albumin with gp60 receptor and SPARC, which promotes the local concentration of loaded albumin nanocarriers in tumors while providing nutrients and energy to facilitate the rapid proliferation of tumor cells.[34,50,51] In addition, some research also suggests that Alb-NPs might act as an inducer of Alb-binding protein aggregation due to their ability to bind and cross-link to multiple receptors.[34] Therefore, the Alb-modified nanoplatform exhibits good tumor-targeted drug delivery.[33,52] Considering the great potential of Alb-NPs in tumor-targeted drug delivery, we attempted to apply it to the delivery of radiosensitizers.

Our investigations revealed that Alb-modified GNPs could achieve the expected tumor-accumulation effect, exhibited good biocompatibility in in vivo circulation, and could be metabolized through the liver and kidney pathways. Moreover, the interaction of GNPs accumulated in the tumor sites and X-rays in vitro improved the damaging effect of ionizing radiation on tumor cells and enhanced the efficacy of radiotherapy. The SER values calculated based on the basic theoretical knowledge of tumor radiobiology also indicated the outstanding radiosensitization effect of the prepared composite nanoplatform. This observation may be attributed to the transcellular pathway and the targeting of Alb-NPs. Although the prepared Alb-GNPs have a relatively larger size than the clinical NPs (<200 nm diameter), their biocompatibility, synergistic antitumor effect, and radiosensitization effect are better than that of other lipid-based and polymer-based NPs. As far as we know, intravenous lipids are quickly removed by the reticuloendothelial system, and high concentrations of surfactants in microemulsions are prone to adverse reactions. The nanomaterials we prepared avoided using toxic materials as much as possible, and no obvious toxicity was observed and detected in vitro and in vivo experiments.

Moreover, the elucidation of mechanisms may promote the understanding of the interaction between GNPs and ionizing radiation. It is generally believed that ionizing radiation-induced DNA damage response includes the

activation of cell cycle checkpoints and DNA damage repair responses; therefore, blocking repair before DNA repair begins can lead to apoptosis or cell death.[3] According to the results of several theoretical and experimental studies, the Au cores of GNPs, as a high atomic number material, may lead to the development of tumor radiosensitization through enhancement of the photoelectric effect, the Compton effect, pair production, and Rayleigh scattering.[4] In this regard, there are several differences between the theoretical and actual measured radiobiological effects. For instance, the strong photoelectric effect of high Z NPs under the KeV level photon beam makes it radiosensitized, while the significant sensitization phenomenon is also observed in the MV level photon beam radiation, although, theoretically, the photoelectric effect cross-section of high-energy photons should be small. Moreover, considering that the high-Z particles promote physical dose deposition, electron pairing effect, and the fluorescence effect, the actual observed sensitization effect is significantly higher than that expected theoretically, especially when using the MV level photon beam.[26]

Similarly, we observed a radiosensitizing effect of Alb-GNPs under MV level X-rays, which produces a greater extent of tumor cell-killing than that predicted theoretically. In the present study, the application of the combination of Alb-GNPs with X-ray led to a greater incidence of DNA double-strand breaks (DSBs) and more numbers of cells arrested in the radiation-sensitive G2/M phase when compared to the application of a single X-ray. This observation can be partially explained by micrometer or nanoscale dose deposition: although the macroscopic dose sensitization effect of NPs for MV level X-rays is small, when NPs accumulate in tumor cells, the microscale sensitization effect can more effectively damage tumor cell DNA and produce a stronger radiosensitizing effect.[26]

Nevertheless, there are some limitations of the present experiment, such as the lack of comparison of different energy levels for radiotherapy, the lack of pharmacokinetic studies, and the lack of verification of multiple tumor models. Moreover, the mechanism of radiosensitization should be explained and described based on the combination of multi-disciplines, which warrants further research and exploration from four different aspects: physics, physical chemistry, chemistry, and biology.

Conclusion

The prepared composite nanomaterial Alb-GNPs exhibited the desired physical and chemical characteristics, including suitable shape, size, charge and colloid stability. As expected, Alb-GNPs showed good biocompatibility and low toxicity, and combined with radiotherapy can effectively increase the radiotherapy injury of tumor cells. Through tumor-bearing mice model, Alb-GNPs combined with radiotherapy can inhibit tumor growth, and delay the median survival period of tumor-bearing mice, demonstrating outstanding radiosensitization and anti-tumor effects. In addition, Alb-GNPs showed superior biosafety both in vitro and in vivo. In general, our study presents an excellent radiosensitizer to boost lung cancer radiotherapy. We believe that Alb-mediated GNPs can be applied to sensitized radiotherapy of other tumor types and that this approach can bring about an encouraging evolution in cancer radiotherapy.

Abbreviations

GNPs, gold nanoparticles; SER, sensitization enhancement ratio; ICRA, International Cancer Research Agency; MRI, magnetic resonance imaging; EPR, enhanced permeability and retention; HSA, human serum albumin; BSA, bovine serum albumin; SPARC, cysteine-rich acid secretory protein; FBS, fetal bovine serum; DMEM, Dulbecco's Modified Eagle's Medium; DMSO, dimethyl sulphoxide; SPF, specific pathogen-free; PDI, polydispersity index; TEM, transmission electron microscope; ICP-OES, inductively coupled plasma spectroscopy; SSD, source skin distance; SF, survival fraction; D_0, lethal dose; D_q, quasi-threshold dose; MV, megavolt; PI, propidium iodide; PBS, phosphate-buffered saline; ICP-AES, inductively coupled plasma-atomic emission spectroscopy; IHC, immunohistochemistry; H&E, haematoxylin and eosin; TUNEL, terminal deoxynucleotidyl transferase-mediated dUTP-biotin nick-end labelling; SD, standard deviation; ROS, reactive oxygen species; CT, computer tomography; DSBs, double-strand breaks; HIF-1α, hypoxia-inducible factor-1α.

Acknowledgments

This work was supported by grants from the Union Project of Luzhou City and the Southwest Medical University (Nos. 14JC0144, 2013LZLY-J40). The figure was created by BioRender.

Disclosure

The authors report no conflicts of interest in this work.

References

1. Siegel R, Miller K, Fuchs H, Jemal A. Cancer statistics, 2022. *CA Cancer J Clin*. 2022;72(1):7–33. doi:10.3322/caac.21708
2. Vinod S, Hau E. Radiotherapy treatment for lung cancer: current status and future directions. *Respirology*. 2020;25(S2):61–71. doi:10.1111/resp.13870
3. Batooei S, Khajeali A, Khodadadi R, Pirayesh Islamian J. Metal-based nanoparticles as radio-sensitizer in gastric cancer therapy. *J Drug Deliv Sci Technol*. 2020;56:101576. doi:10.1016/j.jddst.2020.101576
4. Chen Y, Yang J, Fu S, Wu J. Gold nanoparticles as radiosensitizers in cancer radiotherapy. *Int J Nanomedicine*. 2020;15:9407–9430. doi:10.2147/ijn.S272902
5. Liu Y, Zhang P, Li F, et al. NanoEnhancersMetal-based for future radiotherapy: radiosensitizing and synergistic effects on tumor cells. *RSC Adv*. 2018;8(7):1824–1849. doi:10.7150/thno.22172
6. Song G, Cheng L, Chao Y, Yang K, Liu Z. Emerging nanotechnology and advanced materials for cancer radiation therapy. *Adv Mater*. 2017;29(32):1700996. doi:10.1002/adma.201700996
7. Choi J, Kim G, Cho S, Im H. Radiosensitizing high-Z metal nanoparticles for enhanced radiotherapy of glioblastoma multiforme. *J Nanobiotechnology*. 2020;18(1):122. doi:10.1186/s12951-020-00684-5
8. Zhang Y, Sriramaneni R, Clark P, et al. Multifunctional nanoparticle potentiates the in situ vaccination effect of radiation therapy and enhances response to immune checkpoint blockade. *Nat Commun*. 2022;13(1):4948. doi:10.1038/s41467-022-32645-x
9. Alyani Nezhad Z, Geraily G, Hataminia F, Parwaie W, Ghanbari H, Gholami S. Bismuth oxide nanoparticles as agents of radiation dose enhancement in intraoperative radiotherapy. *Med Phys*. 2021;48(3):1417–1426. doi:10.1002/mp.14697
10. Qin X, Yang C, Xu H, et al. Cell-derived biogenetic gold nanoparticles for sensitizing radiotherapy and boosting immune response against cancer. *Small*. 2021;17(50):e2103984. doi:10.1002/smll.202103984
11. Yang C, Gao Y, Fan Y, et al. Dual-mode endogenous and exogenous sensitization of tumor radiotherapy through antifouling dendrimer-entrapped gold nanoparticles. *Theranostics*. 2021;11(4):1721–1731. doi:10.7150/thno.54930
12. Huo D, Liu S, Zhang C, et al. Hypoxia-targeting, tumor microenvironment responsive nanocluster bomb for radical-enhanced radiotherapy. *ACS Nano*. 2017;11(10):10159–10174. doi:10.1021/acsnano.7b04737
13. Ji C, Zhao M, Wang C, et al. Biocompatible tantalum nanoparticles as radiosensitizers for enhancing therapy efficacy in primary tumor and metastatic sentinel lymph nodes. *ACS Nano*. 2022;16(6):9428–9441. doi:10.1021/acsnano.2c02314
14. Peng C, Liang Y, Su N, et al. Dual nanoenzymes loaded hollow mesoporous organotantalum nanospheres for chemo-radio sensitization. *J Control Release*. 2022;347:369–378. doi:10.1016/j.jconrel.2022.05.018
15. Song G, Chen Y, Liang C, et al. Catalase-loaded TaOx nanoshells as bio-nanoreactors combining high-Z element and enzyme delivery for enhancing radiotherapy. *Adv Mater*. 2016;28(33):7143–7148. doi:10.1002/adma.201602111
16. Chen Y, Song G, Dong Z, et al. Drug-loaded mesoporous tantalum oxide nanoparticles for enhanced synergetic chemoradiotherapy with reduced systemic toxicity. *Small*. 2017;13(8). doi:10.1002/smll.201602869
17. Zhang P, Marill J, Darmon A, Mohamed Anesary N, Lu B, Paris S. NBTXR3 radiotherapy-activated functionalized hafnium oxide nanoparticles show efficient antitumor effects across a large panel of human cancer models. *Int J Nanomedicine*. 2021;16:2761–2773. doi:10.2147/ijn.S301182
18. Zhao J, Liu P, Ma J, et al. Enhancement of radiosensitization by silver nanoparticles functionalized with polyethylene glycol and aptamer As1411 for glioma irradiation therapy. *Int J Nanomedicine*. 2019;14:9483–9496. doi:10.2147/ijn.S224160
19. Tremi I, Spyratou E, Souli M, et al. Requirements for designing an effective metallic Nanoparticle (NP)-Boosted Radiation Therapy (RT). *Cancers*. 2021;13(13):3185. doi:10.3390/cancers13133185
20. Cui L, Her S, Borst G, Bristow R, Jaffray D, Allen C. Radiosensitization by gold nanoparticles: will they ever make it to the clinic? *Radiother Oncol*. 2017;124(3):344–356. doi:10.1016/j.radonc.2017.07.007
21. Dimitriou N, Tsekenis G, Balanikas E, et al. Gold nanoparticles, radiations and the immune system: current insights into the physical mechanisms and the biological interactions of this new alliance towards cancer therapy. *Pharmacol Ther*. 2017;178:1–17. doi:10.1016/j.pharmthera.2017.03.006
22. Her S, Jaffray D, Allen C. Gold nanoparticles for applications in cancer radiotherapy: mechanisms and recent advancements. *Adv Drug Deliv Rev*. 2017;109:84–101. doi:10.1016/j.addr.2015.12.012
23. Silva F, Paulo A, Pallier A, et al. Dual imaging gold nanoplatforms for targeted radiotheranostics. *Materials*. 2020;13(3):513. doi:10.3390/ma13030513
24. Schuemann J, Berbeco R, Chithrani D, et al. Roadmap to clinical use of gold nanoparticles for radiation sensitization. *Int J Radiat Oncol Biol Phys*. 2016;94(1):189–205. doi:10.1016/j.ijrobp.2015.09.032
25. Dobešová L, Gier T, Kopečná O, et al. Incorporation of low concentrations of gold nanoparticles: complex effects on radiation response and fate of cancer cells. *Pharmaceutics*. 2022;14(1):166. doi:10.3390/pharmaceutics14010166
26. Kempson I. Mechanisms of nanoparticle radiosensitization. *Wiley Interdiscip Rev*. 2021;13(1):e1656. doi:10.1002/wnan.1656
27. Tremi I, Havaki S, Georgitsopoulou S, et al. Biological response of human cancer cells to ionizing radiation in combination with gold nanoparticles. *Cancers*. 2022;14(20):5086. doi:10.3390/cancers14205086
28. Karimi M, Bahrami S, Ravari S, et al. Albumin nanostructures as advanced drug delivery systems. *Expert Opin Drug Deliv*. 2016;13(11):1609–1623. doi:10.1080/17425247.2016.1193149

29. Misak H, Asmatulu R, Gopu J, et al. Albumin-based nanocomposite spheres for advanced drug delivery systems. *Biotechnol J*. 2014;9(1):163–170. doi:10.1002/biot.201300150
30. Jahanban-Esfahlan A, Dastmalchi S, Davaran S. A simple improved desolvation method for the rapid preparation of albumin nanoparticles. *Int J Biol Macromol*. 2016;91:703–709. doi:10.1016/j.ijbiomac.2016.05.032
31. Tang X, Wang G, Shi R, et al. Enhanced tolerance and antitumor efficacy by docetaxel-loaded albumin nanoparticles. *Drug Deliv*. 2016;23 (8):2686–2696. doi:10.3109/10717544.2015.1049720
32. Van de Sande L, Cosyns S, Willaert W, Ceelen W. Albumin-based cancer therapeutics for intraperitoneal drug delivery: a review. *Drug Deliv*. 2020;27(1):40–53. doi:10.1080/10717544.2019.1704945
33. An F, Zhang X. Strategies for preparing albumin-based nanoparticles for multifunctional bioimaging and drug delivery. *Theranostics*. 2017;7 (15):3667–3689. doi:10.7150/thno.19365
34. Lin T, Zhao P, Jiang Y, et al. Blood-brain-barrier-penetrating albumin nanoparticles for biomimetic drug delivery via albumin-binding protein pathways for antiglioma therapy. *ACS Nano*. 2016;10(11):9999–10012. doi:10.1021/acsnano.6b04268
35. Liu S, Piao J, Liu Y, et al. Radiosensitizing effects of different size bovine serum albumin-templated gold nanoparticles on H22 hepatoma-bearing mice. *Nanomedicine*. 2018;13(11):1371–1383. doi:10.2217/nnm-2018-0059
36. Bolaños K, Kogan M, Araya E. Capping gold nanoparticles with albumin to improve their biomedical properties. *Int J Nanomedicine*. 2019;14:6387–6406. doi:10.2147/ijn.S210992
37. Zhang Y, Huang F, Ren C, et al. Enhanced radiosensitization by gold nanoparticles with acid-triggered aggregation in cancer radiotherapy. *Adv Sci*. 2019;6(8):1801806. doi:10.1002/advs.201801806
38. Goswami N, Luo Z, Yuan X, Leong DT, Xie J. Engineering gold-based radiosensitizers for cancer radiotherapy. *Mater Horiz*. 2017;4(5):817–831. doi:10.1039/c7mh00451f
39. Zhen W, Weichselbaum R, Lin W. Nanoparticle-mediated radiotherapy remodels the tumor microenvironment to enhance antitumor efficacy. *Adv Mater*. 2022;e2206370. doi:10.1002/adma.202206370
40. Alle M, Sharma G, Lee S, Kim J. Next-generation engineered nanogold for multimodal cancer therapy and imaging: a clinical perspectives. *J Nanobiotechnology*. 2022;20(1):222. doi:10.1186/s12951-022-01402-z
41. Wen S, Ovais M, Li X, et al. Tailoring bismuth-based nanoparticles for enhanced radiosensitivity in cancer therapy. *Nanoscale*. 2022;14 (23):8245–8254. doi:10.1039/d2nr01500e
42. Luan S, Xie R, Yang Y, et al. Acid-responsive aggregated gold nanoparticles for radiosensitization and synergistic chemoradiotherapy in the treatment of esophageal cancer. *Small*. 2022;18(19):e2200115. doi:10.1002/smll.202200115
43. Yu Y, Yang T, Sun T. New insights into the synthesis, toxicity and applications of gold nanoparticles in CT imaging and treatment of cancer. *Nanomedicine*. 2020;15(11):1127–1145. doi:10.2217/nnm-2019-0395
44. Wei J, Li P, Zhang H, Zhu R. Preparation of BSA-coated Au nanoparticles contrast agent and its application in PETCT imaging. *Cell Mol Biol*. 2022;68(3):158–170. doi:10.14715/cmb/2022.68.3.19
45. López-Valverde J, Jiménez-Ortega E, Leal A. Clinical feasibility study of gold nanoparticles as theragnostic agents for precision radiotherapy. *Biomedicines*. 2022;10(5):1214. doi:10.3390/biomedicines10051214
46. Haume K, Rosa S, Grellet S, et al. Gold nanoparticles for cancer radiotherapy: a review. *Cancer Nanotechnol*. 2016;7(1):8. doi:10.1186/s12645-016-0021-x
47. Al-Abd A, Aljehani Z, Gazzaz R, et al. Pharmacokinetic strategies to improve drug penetration and entrapment within solid tumors. *J Control Release*. 2015;219:269–277. doi:10.1016/j.jconrel.2015.08.055
48. Chen Q, Feng L, Liu J, et al. Intelligent albumin-MnO2 nanoparticles as pH-/H2 O2 -responsive dissociable nanocarriers to modulate tumor hypoxia for effective combination therapy. *Adv Mater*. 2016;28(33):7129–7136. doi:10.1002/adma.201601902
49. Wang Y, Yang T, Ke H, et al. Smart albumin-biomineralized nanocomposites for multimodal imaging and photothermal tumor ablation. *Adv Mater*. 2015;27(26):3874–3882. doi:10.1002/adma.201500229
50. Paul M, Itoo A, Ghosh B, Biswas S. Current trends in the use of human serum albumin for drug delivery in cancer. *Expert Opin Drug Deliv*. 2022;19(11):1449–1470. doi:10.1080/17425247.2022.2134341
51. Cho H, Jeon S, Ahn C, Shim M, Kim K. Emerging albumin-binding anticancer drugs for tumor-targeted drug delivery: current understandings and clinical translation. *Pharmaceutics*. 2022;14(4):728. doi:10.3390/pharmaceutics14040728
52. Wang H, Wu J, Xu L, Xie K, Chen C, Dong Y. Albumin nanoparticle encapsulation of potent cytotoxic therapeutics shows sustained drug release and alleviates cancer drug toxicity. *Chem Commun*. 2017;53(17):2618–2621. doi:10.1039/c6cc08978j